Tungsten-Doped Titanium Dioxide in the Rutile Structure: Theoretical Considerations

Masoud Aryanpour,[†,‡] Roald Hoffmann,[*,‡] and Francis J. DiSalvo[‡]

Department of Geosciences, The Pennsylvania State University, University Park, Pennsylvania 16802, and Department of Chemistry and Chemical Biology, Baker Laboratory, Cornell University, Ithaca, New York 14850

Received February 4, 2009. Revised Manuscript Received March 5, 2009

Tungsten-doped titanium dioxide has the potential to replace conventional carbon black in catalyst support applications. In this paper, structural and electronic properties of W-doped rutile are theoretically studied. Lattice parameters as well as W−W pairing in models for a range of doping are calculated and match well with the experimental results. W doping leads to in-plane expansion and *c*-axis contraction in the rutile structure. The pairing of tungsten atoms is a Peierls-type distortion, resulting in less cluttering of bands around the Fermi energy. Our computational finding of paired structures as energetically more stable is in agreement with the literature on similar systems. W-doped rutile is conducting at both high and low doping levels; the states involved near the Fermi level are predominantly W(5d).

1. Introduction

Our unabated demand for energy has motivated much research and industrial investment to improve and/or replace conventional combustive power sources. The shift to alternative sources is accelerated by pollution issues and environmental considerations.[1,2] As noncombustive means of power generation already exist, the grand current task is to reduce the overall cost of both power production and maintenance with these methods. Most promising alternative energy sources, such as fuel cells and batteries, aim to directly convert chemical energy into electrical energy. At the heart of the challenges facing us lies the need for better materials that could increase overall energy production through improved chemistry based on their superior functionality.

Focusing on the electrodes of proton-exchange membrane (PEM) fuel cells, there is room for improvement of both the catalyst and its support. For the catalyst, one wishes to reduce the overpotential of the oxygen reduction reaction, and to use materials cheaper than platinum-based catalysts. The catalyst support must fulfill other requirements:[2] it must (i) be conductive by more than 1 S/cm, (ii) be stable up to at least 1.5 V with respect to the standard hydrogen electrode, and (iii) be stable in the acidic, low pH environment of PEM fuel cells.

At least in automotive applications of PEM fuel cells, carbon black is currently the main material for catalyst support. Although showing the primary features of a good support, carbon is only kinetically persistent, not thermodynamically stable, under fuel cell operating conditions. It corrodes at low pH and high electrode potential according to the following redox reaction

$$C + 2H_2O \rightarrow CO_2 + 4H^+ + 4e^- \quad E_0 = 0.2\ V \quad (1)$$

On the basis of experimental measurements and a simple model, Mathias et al.[2] showed that at 0.9 V and after several thousand hours, 5% of carbon is lost in a standard Pt/C electrode. Similar studies estimate 15% carbon weight loss at 1.2 V and after only 20 hours of operation. This much weight loss is not tolerable in automotive applications, because more than 5% loss leads to an unacceptable decrease in the cell performance. The same authors also studied a sample of 30% Pt alloy on graphitized carbon as the electrode. Although it exhibits improved performance in terms of carbon loss, this material still has to be optimized if it is to become practical.

In searching for alternative support materials, one realizes that at a potential of 1.2 V and above in acidic aqueous media, all metallic elements should dissolve. This is evident from the Pourbaix diagrams, a way to gauge the stability of phases under different pH and electrochemical conditions.[3] To avoid corrosion, one is naturally led to consider other materials such as metal oxides, which resist (further) oxidation and may be stable under fuel cell operating conditions. In particular, the Pourbaix diagram for Ti suggests that titanium dioxide (TiO_2) is a stable material over the pH−potential range of interest and thus is a potential candidate to replace carbon black. Note, however, that in the presence of some specific anions, such as sulfate, or in its hydrated form, TiO_2 may become soluble or corrode.[4]

* Corresponding author. E-mail: rh34@cornell.edu.
† The Pennsylvania State University.
‡ Cornell University.

(1) Carrette, L.; Friedrich, K. A.; Stimming, U. *Fuel Cells* **2001**, *1* (1), 320–324.
(2) Mathias, M. F.; Makharia, R.; Gasteiger, H. A.; Conley, J. J.; Fuller, T. J.; Gittleman, C. J.; Kocha, S. S.; Miller, D. P.; Mittelsteadt, C. K.; Xie, T.; Yan, S. G.; Yu, P. T. *J. Electrochem. Soc. Interface* **2005**, *14* (3), A970−A977.
(3) Pourbaix, M. *Atlas of Electrochemical Equilibria in Aqueous Solutions*; NACE International: Houston, 1974.
(4) Kolenko, Y. V.; Burukhin, A. A.; Churagulov, B. R.; Oleinikov, N. N. *Inorg. Mater.* **2004**, *40*, 822–828.

10.1021/cm900329k CCC: $40.75
Published on Web 04/07/2009

TiO_2 is an excellent model system, widely studied both experimentally and theoretically.[5] The reader is referred to the rich literature on titanium dioxide, for instance, on its structure and electronic properties,[6] synthesis,[7] surface characteristics and photocatalysis,[5,8] stability and reactivity,[9] and interaction with organic molecules.[5,10−13] To realize the significance of its wide industrial applications, one can mention the use of TiO_2 in paints,[10,14] optics,[15−17] electronics,[18] sensors,[19,20] and photocatalysis.[21,22]

The three most common (out of seven) TiO_2 polymorphs are anatase, rutile, and brookite.[23] Brookite reverts to the rutile structure above 750 °C. Although experiments report rutile to be slightly (by about 0.1 eV) more stable than anatase,[24] computations find a lower energy for anatase instead.[25] Both rutile and anatase have a tetragonal structure and are chemically stable semiconductors with a large 3.0−3.5 eV band gap.[25,26] Thus TiO_2 meets the stability criterion to be used as catalyst support. However, it is an insulator, and conductivity must be attained by doping, for example, by cation substitution or by oxygen vacancies.

Doping TiO_2 to modify its properties is yet another area rich in interest in both research and practical applications.[5] Anatase and rutile structures have been doped with not only transition metals such as Mn, Fe, Co, Ni, Mo, Cr, Nb, W, and Re[27−29] but also main group elements such as B, N, and F.[30−32] The focus of this work is the change in geometry and conductivity of TiO_2 in the rutile structure upon tungsten doping, because recent unpublished work here at Cornell suggests that this material may have sufficient electrochemical stability to be a possible catalyst support. WO_2 has a distorted rutile structure with W−W pair bonding and it is a conductive material;[33] however, it is stable over only a narrow range of potential near −0.1 V.[3] Apparently, when doped into TiO_2 at low enough levels, the W is protected from corrosion. Further W doping stabilizes the rutile form of TiO_2, in accord with other experimental results.[24]

In this paper, we first revisit the atomic and electronic structure of rutile, which lays the foundation for studying W-doped structures. The effect of doping on the geometry and electronic structure is examined and compared with the experimental results. Next, we explore the relationship between the structural readjustments induced by allowing the formation of W−W pairs, as in pure WO_2. The discussions are based on energetics and band structures obtained by quantum calculations and ab initio Molecular Dynamics (MD) simulations. Some of the graphics for the crystals presented in this paper have been created using XCrySDen.[34]

2. Rutile Structure

Rutile TiO_2 crystallizes in the $P4_2/mnm$ space group. Each titanium atom is nearly octahedrally coordinated with oxygen atoms, and each oxygen atom in turns bonds with three metal atoms. Chains of octahedra run along the *c* axis of the crystal, sharing equatorial edges with each other (Figure 1). The four equatorial Ti−O bonds of length 1.9485 are slightly shorter than the two apical bonds of length 1.9800.[35,36] The rutile lattice constants, obtained by X-ray scattering techniques,[35] are $a = b = 4.59366$, and $c = 2.95868$. There are two formula units in the unit cell. The band structure of the rutile model in Figure 1a is shown in Figure 2. These band calculations were performed on the optimized structure using the VASP code[37−39] and PAW-GGA pseudopotentials[40,41] with a cutoff energy of 36.75 Ry. The energy levels here, which are almost identical with previously published results,[25,42] can be understood in orbital details as follows: the unit cell has $Z = 2$, $(TiO_2)_2$. The four lowest bands (below

(5) Diebold, U. *Surf. Sci. Rep.* **2003**, *48*, 53–229.
(6) Hoffmann, R. *Solids and Surfaces: A Chemist's View of Bonding in Extended Structures*; Wiley-VCH: New York, 1988.
(7) Chen, X.; Mao, S. S. *Chem. Rev.* **2007**, *107*, 2891–2959.
(8) Bredow, T.; Giordano, L.; Cinquini, F.; Pacchioni, G. *Phys. Rev. B* **2004**, *70*, 035419.
(9) Vittadini, A.; Casarin, M.; Selloni, A. *Theor. Chem. Acc.* **2007**, *117* (5−6), 663–671.
(10) Braun, J. H.; Baidins, A.; Marganski, R. E. *Prog. Org. Coat.* **1992**, *20* (2), 105–138.
(11) Zapol, P.; Curtiss, L. A. *J. Comput. Theor. Nanosci.* **2007**, *4* (2), 222–230.
(12) Ballarini, N.; Cavani, F.; Di Memmo, S.; Zappoli, F.; Marion, P. *Catal. Today* **2004**, *89* (3), 264–270.
(13) Calatayud, M.; Markovits, A.; Menetrey, M.; Mguig, B.; Minot, C. *Catal. Today* **2005**, *85* (2−4), 125.
(14) Lim, B. C.; Thomas, N. L.; Sutherland, I. *Prog. Org. Coat.* **2008**, *62* (2), 123–128.
(15) Seifering, K. L.; Griffin, G. L. *J. Electrochem. Soc.* **1990**, *137* (4), 1206–1208.
(16) Penard, A. L.; Gacoin, T.; Boilot, J. P. *Acc. Chem. Res.* **2007**, *40* (9), 895–902.
(17) Alvaro, M.; Carbonell, E.; Atienzar, P.; Garcia, H. *Chemphyschem* **2006**, *7* (9), 1996–2002.
(18) Masuda, Y.; Sugiyama, T.; Lin, H. *Thin Solid Films* **2001**, *382* (1−2), 153–157.
(19) Steele, J. J.; van Popta, A. C.; Hawkeye, M. M.; Sit, J. C.; Brett, M. J. *Sens. Actuators, B* **2006**, *120* (1), 213–219.
(20) Teleki, A.; Pratsinis, S. E.; Kalyanasundaram, K.; Gouma, P. I. *Sens. Actuators, B* **2006**, *119* (2), 683–690.
(21) Anpo, M.; Yamishita, H.; Ichihashi, Y.; Ehara, S. *J. Electroanal. Chem.* **1995**, *396* (1−2), 21–26.
(22) Dey, G. R. *J. Nat. Gas Chem.* **2007**, *16* (3), 217–226.
(23) Reyes-Coronado, D.; Rodriguez-Gattorno, G.; Espinosa-Pesqueira, M. E.; Cab, C.; de Coss, R.; Oskam, G. *Nanotechnology* **2008**, *19* (14), 145605.
(24) West, R. C. *Handbook of Chemistry and Physics*; CRC Press: Boca Raton, FL, 1986.
(25) Mikami, M.; Nakamura, S.; Kiato, O.; Arakawa, H.; Gonze, X. *Jpn. J. Appl. Phys.* **2000**, *39*, L847–850.
(26) Ashour, A. *Surf. Rev. Lett.* **2006**, *13* (1), 87–92.
(27) Murugan, P.; Belosludov, R. V.; Mizuseki, H.; Nishimatsu, T.; Fukumura, T.; Kawasaki, M.; Kawazoe, Y. *J. Appl. Phys.* **2006**, *99* (8), 08M105.
(28) Park, M. S.; Kwon, S. K.; Min, B. I. *Phys. Rev. B* **2002**, *65* (16), 161201.
(29) Weng, H. M.; Yang, X. P.; Dong, J. M.; Mizuseki, H.; Kawasaki, M.; Kawazoe, Y. *Phys. Rev. B* **2004**, *69* (12), 125219.
(30) Burda, C.; Lou, Y.; Chen, X.; Samia, A. C. S.; Stout, J.; Gole, J. L. *Nano Lett.* **2003**, *3* (8), 1049–1051.
(31) Todorova, N.; Giannakopoulou, T.; Romanos, G.; Vaimakis, T.; Yu, J. G.; Trapalis, C. *Int. J. Photoenergy* **2008**, 534038.
(32) Liu, G.; Zhao, Y.; Sun, C.; Li, F.; Lu, G. Q.; Cheng, H. M. *Angew. Chem., Int. Ed.* **2008**, *47* (24), 4516–4520.
(33) Palmer, D. J.; Dickens, P. G. *Acta Crystallogr., Sect. B* **1979**, *35*, 2199–2201.
(34) Kokalj, A. *Comput. Mater. Sci.* **2003**, *28*, 155–168.
(35) Abrahams, S. C.; Bernstein, J. L. *J. Chem. Phys.* **1971**, *55*, 3206.
(36) Mak, T. C. W. and Zhou, G. D. *Crystallography in Modern Chemistry*; John Wiley and Sons Inc.: New York, 1992.
(37) Kresse, G.; Hafner, J. *Phys. Rev. B* **1993**, *47*, RC558.
(38) Kresse, G.; Furthmüller, J. *Comput. Mater. Sci.* **1996**, *6*, 15.
(39) Furthmüller, J. *Phys. Rev. B* **1996**, *54*, 11169.
(40) Blöchl, P. E. *Phys. Rev. B* **1994**, *50*, 17953.
(41) Kresse, G.; Joubert, J. *Phys. Rev. B* **1999**, *59*, 1758.
(42) Labat, F.; Baranek, P.; Domain, C.; Minot, C.; Adamo, C. *J. Chem. Phys.* **2007**, *126*, 154703.

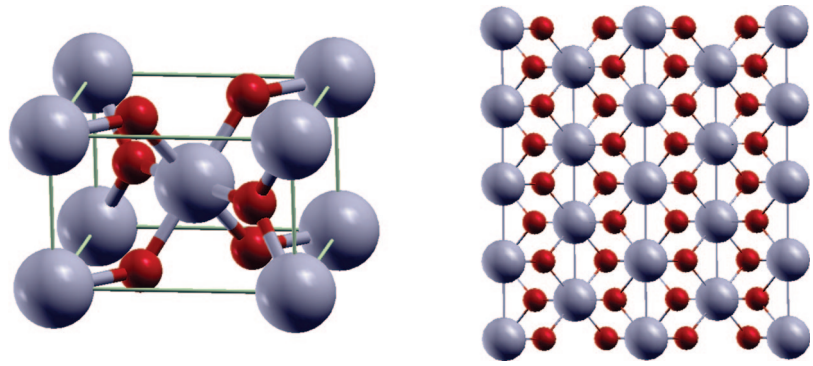

Figure 1. Rutile structure with larger spheres representing Ti atoms: (a) conventional unit cell consisting of two TiO_2 formula units, (b) one view of extended structure, showing the edge-sharing octahedral chains (O atoms are the smaller spheres).

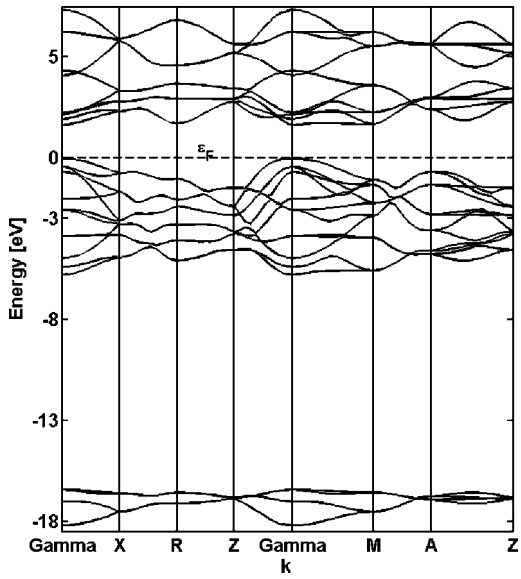

Figure 2. Band structure of rutile with two TiO_2 formula units per unit cell as in Figure 1a.

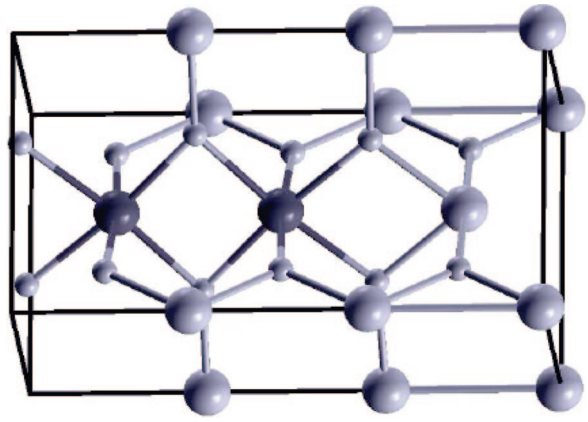

Figure 3. Model structure for $Ti_{0.67}W_{0.33}O_2$. Darker spheres represent tungsten atoms, whereas the smaller spheres represent oxygen.

−15 eV) correspond to states dominated by O(2s) orbitals, the valence bands are dominated by the 12 O(2p) levels. There follows a gap to the conduction bands, predominantly based on the 3d orbitals of the Ti atoms.

Although there is not a perfect octahedral environment of Ti atoms in rutile, the coordination of Ti is close to ideal. The classic crystal field splitting of three-below-two states is demonstrated clearly by 6 levels of t_{2g} and four levels of e_g character.[6] The direct band gap at the Γ point is ∼1.86 eV, which is very close to ∼1.88 reported by Mikami et al.[25] but much smaller than the experimental value of 3.0 eV.[43] Such underestimation of band gap by LDA and GGA is a well-known trend in pure DFT calculations.[25,44] Labat et al.[42] showed that hybrid functionals, mixing HF exchange with PBE exchange-correlation, can calculate larger gaps for rutile, more in accord with the experimental values.

Table 1. Effect of W-Doping on Rutile Structure Obtained by DFT Calculations in This Work, And Measured by X-ray Diffraction Pattern[46]

	calculations					experiments	
W-doping (%)	0 (rutile)	20	25	33	50	0 (rutile)	30
a (Å)	4.66	4.72	4.73	4.76	4.82	4.59	4.68
$\Delta a(\%)^a$	0.0	1.36	1.62	2.11	3.55	0.0	1.96
c (Å)	2.97	2.94	2.93	2.92	2.85	2.96	2.90
$\Delta c(\%)^a$	0.0	−0.74	−1.03	−1.55	−3.82	0.0	−1.79
V (Å^3)	64.32	65.58	65.72	66.00	66.30	62.42	63.66
$\Delta v(\%)^a$	0.0	1.97	2.18	2.61	3.08	0.0	1.99

[a] Relative change with respect to the corresponding value in the pure rutile structure.

3. W-Doping Effects on Rutile Structure

The empirical crystal radius of a titanium atom is 1.45 in the elemental α-Ti structure and 0.61 in ionic form as Ti^{4+}. Close to these values are corresponding radii for tungsten: 1.37 and 0.66, respectively. Thus one can expect that upon doping, tungsten atoms substitute titanium atoms in rutile at octahedral sites without substantially modifying the underlying crystal structure, but not without electronic consequences, as we will see.

Although the subject of this paper is a theoretical analysis of the electronic behavior of the doped rutile phase $Ti_{(1-x)}W_xO_2$, a short description of the synthesis of this oxide is in order. Samples are prepared in 5−10 g batches at values of x between 0 and 0.5 by combining the appropriate stoichiometric ratios of the reactants and heating to 1100 °C in a sealed, evacuated silica tube for 8−10 days

$$(1 - x)TiO_2 + \frac{2}{3}xWO_3 + \frac{x}{3}W \rightarrow Ti_{(1-x)}W_xO_2 \quad (2)$$

(43) Pascual, J.; Camassel, J.; Mathieu, H. *Phys. Rev. B* **1978**, *18*, 5606.
(44) Asahi, R.; Taga, Y.; Mannstadt, W.; Freeman, A. J. *Phys. Rev. B* **2000**, *61*, 7459.

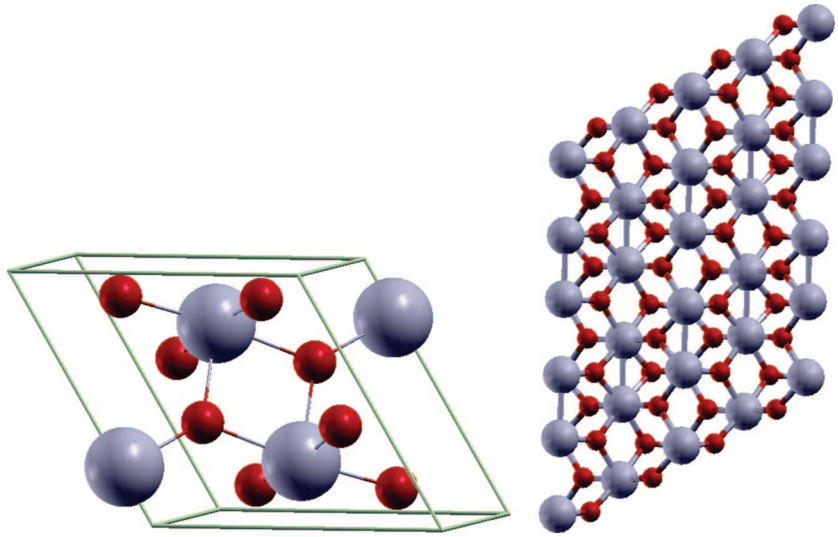

Figure 4. Crystal structure of WO_2 in space group $P2_1/c$. Unit cell at left, extended piece of structure at right. Notice the W pairing, and compare with Figure 1 right to see the small perturbation on the rutile structure.

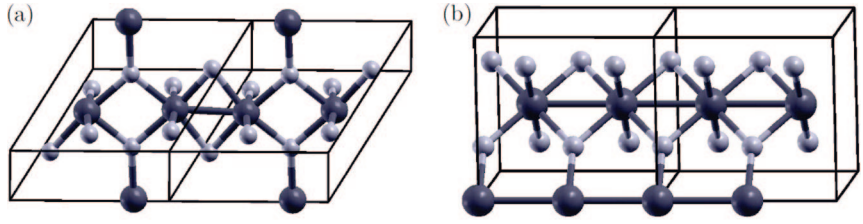

Figure 5. Two unit cells each containing four WO_2 formulas for two space groups: (a) $P2_1/c$, and (b) $P4_2/mnm$ (W atoms are larger).

Table 2. Optimized Lattice Parameters of WO_2 for the Two Models in Figure 5, Measured by Powder Neutron Diffraction,[33] and Obtained by DFT Calculations (VASP and Quantum-ESPRESSO Codes)

	space group				
	$P2_1/c$			$P4_2/mnm$	
	exp	VASP	quantum-ESPRESSO	VASP	Quantum-ESPRESSO
a (Å)	5.56	5.56	5.60	4.93	4.98
b (Å)	4.90	4.91	4.94	4.93	4.98
c (Å)	5.57	5.67	5.70	5.39	5.39
β (deg)	120.47	120.40	120.58	90.00	90.00
W−W (Å)[a]	2.48	2.48	2.51	2.70	2.69
W−W (Å)[b]	3.10	3.10	3.10	2.70	2.69

[a] Corresponds to the metal−metal short distance in paired structures. [b] Corresponds to the metal−metal long distance in paired structures.

Approximately 10 mg of C_6Cl_6 is added to the reaction mixture to allow chemical vapor transport to increase the kinetics of reaction.[45] C_6Cl_6 decomposes at high temperature to provide chlorine that promotes the formation of volatile Ti and W species at the reaction temperature.

Theoretically, we study rutile structures doped with 20, 25, 33, and 50% of tungsten, as well as WO_2 itself. There are a number of ways to model the doping in a translationally ordered structure (by itself a model for the likely disordered real doped crystal). The approach we have chosen is to leave one chain purely titanium, and into the other chain to place two adjacent W atoms plus a sufficient number of Ti atoms to complete the crystalline structure. The resulting cell is doubled in size compared to the minimum cell. The exception is the 50% doping case, which is modeled by two separate chains of tungsten and titanium; the unit cell is as large as the minimal cell. Figure 3 illustrates the supercell for 33% doping, where four titanium, two tungsten, and twelve oxygen atoms in the model generate the desired stoichiometry. Our choice for implanting two W atoms, instead of only one, was to allow anticipated W−W interaction to occur.

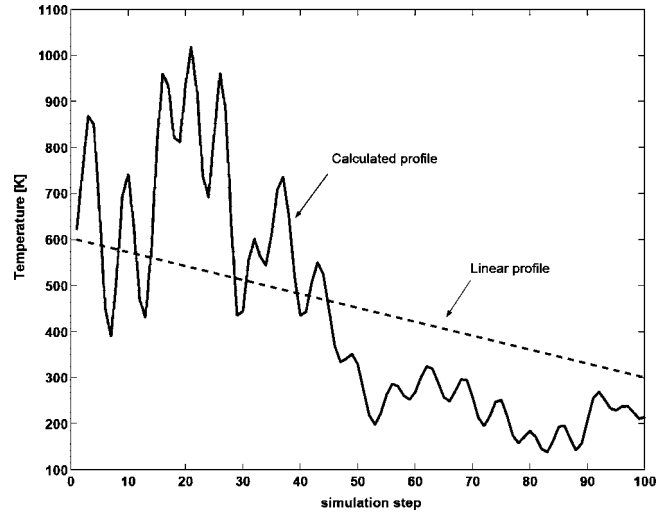

Figure 6. Temperature profile of annealing simulation performed on WO_2 model of Figure 5b.

First, some gross characteristics of the effect of doping: in Table 1, lattice parameters for doped rutile are presented as they emerge from our DFT calculations and experimental measurements.[46] Previous theoretical values of a and c range

(45) Schäfer, H. *Chemical Transport Reactions*; Academic Press: New York, 1964.

Table 3. Formation of Pair in the Structure of WO_2:*P*4$_2$/*mnm* after 100 Steps of ab initio MD Simulations and Retained during a Final Unit-Cell Optimization

	after 100 MD steps	optimized cell
a (Å)	4.59	4.89
c (Å)	5.92	5.52
W−W (Å)	2.73	2.52
W−W′ (Å)	3.19	3.00
ΔE (eV)[†]	1.30	1.10

[†] With respect to paired *P*2$_1$/*c* structure of Figure 4a.

Table 4. Optimized Lattice Parameters of $Ti_{(1-x)}W_xO_2$ ($x = 0.33$, 0.5) in *P*4$_2$/*mnm* Morphology Obtained by DFT Calculations[a]

	$[Ti_{0.67}W_{0.33}O_2]_{12}$		$[Ti_{0.5}W_{0.5}O_2]_4$	
	Opt.	MD + Opt.	Opt.	MD + Opt.
a (Å)	4.76	4.76	4.75	4.72
b (Å)	4.76	4.76	4.75	4.73
c (Å)	17.51	17.54	5.74	5.79
W−W (Å)	2.68	2.65	2.87	2.63
W−W′ (Å)	3.15	3.16	2.87	3.16
W−Ti (Å)	3.03	3.05	–	–
Ti−Ti [Å]	2.91	2.94	2.87	2.89
ΔE (eV)	0.00[b]	−0.02	0.00[b]	−0.36

[a] Interatomic distances are between metal atoms residing on one chain, for which the average is reported whenever more than one value is present. [b] Energy reference level.

between 4.528 and 4.653 and 2.918 and 2.983, respectively.[25] Experimental values for the same lattice parameters are 4.593 and 2.958.[25,47] We calculate 4.658 and 2.965, respectively. The calculations agree with the literature results. If one compares the theoretical relative changes for 33% doping with the experimental relative changes for 30% doping, the general agreement is excellent: both show about a 2% increase in *a*, more than 1.5% decrease in *c*, and approximately 2% increase in unit-cell volume.

These checks done, let us consider the trend of the structural change as the doping percentage increases from 0 to 50. In $Ti_{0.5}W_{0.5}O_2$, the in-plane expansion of the crystal is about 3%, close to the *c*-axis shrinkage. Because the crystal expands in two horizontal directions *a* and *b* but shrinks along the vertical axis *c* by more or less the same amount, the overall change in volume is positive too. Intermediate doping percentages between 0 and 50 lead to corresponding intermediate changes.

The observed reduction of lattice constant *c*, along the vertical axis containing two adjacent tungsten atoms, is suggestive of W−W bonding. Our calculations reveal that the interatomic W−W distance in the doped vertical chain is indeed consistently shorter than the Ti−W distance, for example 2.7 versus 3.0 in 33% doping. The noted W−W distance reduction is important, and greater than one might expect from considerations of atomic or ionic radii.

It should be noted that once W pairing is explicitly studied (see below), there is a secondary reduction in the unit cell *a* dimension. That is, the *a* dimension of the rutile structure increases on incorporation of W into the lattice, but then diminishes again once the W atoms are allowed to pair.

Indeed, there are good electronic reasons for the W−W pairing in these structures. To see these, we need to stand back for a moment and look at the geometry of WO_2, and more generally at pairing in extended MO_2 phases and MO_4 chains. Such pairing as one sees in WO_2 makes sense. Consider an infinite one-dimensional, edge-shared octahedral MO_4 chain. Such chains are found in common oxides such as TiO_2, WO_2, NbO_2, etc. If the metal is (formally) completely oxidized (Ti^{4+} in TiO_2), there is no reason to expect a pairing distortion. For a d^1 metal (e.g., V^{4+} in VO_2) one electron per metal enters the t_{2g}-like band. The half-occupied σ-type band made up from d_{z^2}-type orbitals (*z* is the chain axis) drives a Peierls distortion to a paired structure. In that structure, one finds alternating short and long M−M distance, formally alternating M−M bonds and no bonds.[48,49] This situation for vanadium dioxide is very well analyzed in the literature.[50−52] In WO_2 a similar pairing distortion is expected and observed; it has been explored by Burdett in some detail.[49] Its nature is more complicated; we will return to a discussion of the coupling of the pairing and the conductivity that remains below.

4. WO_2 Structure

At this point, we step back and review what we know about WO_2 itself. Analysis of powder neutron diffraction data shows that WO_2 crystallizes in space group *P*2$_1$/*c* with $a = 5.563$, $b = 4.896$, $c = 5.663$, and $\beta = 120.47°$ at 298 K.[33] The *P*2$_1$/*c* structure, illustrated in Figure 4, is a variant on the rutile structure *P*4$_2$/*mnm* shown in Figure 1b. The difference between the two structures is subtle; both feature chains of metal-centered octahedra,and three-coordinated oxygen atoms, but the unit cell in *P*2$_1$/*c* is monoclinic and not tetragonal as in *P*4$_2$/*mnm*. Examination of three-dimensional models shows small distortions due to W−W pairing in WO_2. The removal of certain symmetry elements leads to a unit-cell reorientation in the new space group. That difference appears more severe than the actual small motions of the atoms involved (compare the right-hand sides of Figures 1 and 4).

There is significant pairing of metal atoms in the WO_2 structure. The W−W bond lengths in WO_2:*P*2$_1$/*c* alternate between short (2.475) and long (3.096) along one axis.[33] Our DFT optimization calculations of WO_2:*P*2$_1$/*c* reproduce this alternation, its metrics in good agreement with experiment. In contrast, calculations of WO_2 in the *P*4$_2$/*mnm* rutile structure did not lead to a pairing instability (nor to deformation to the monoclinic form): all W−W distances along metal chains come out equal; small perturbations toward pairing increase the system energy. This puzzling result is explored next.

5. Pair Formation in WO_2 and W-Doped Rutile

To allow for pairing between metal atoms in a model for WO_2, the computational cell has to contain at least four

(46) Ranjan, C. Munie, S. Hunting, J. DiSalvo, F. J. **2009**, to be published.
(47) Burdett, J. K.; Hughbanks, T.; Miller, G. J.; Richardson, J. W.; Smith, J. V. *J. Am. Chem. Soc.* **1987**, *109*, 3639–3646.
(48) Whangbo, M. H.; Foshee, M. J. *Inorg. Chem.* **1981**, *20*, 113–118.
(49) Burdett, J. K. *Inorg. Chem.* **1985**, *24*, 2244–2253.
(50) Gupta, M.; Freeman, A. J.; Ellis, D. E. *Phys. Rev. B.* **1977**, *16*, 3338.
(51) Wentzcovitch, R. M.; Martin, J. L.; Price, G. D. *Phys. Rev. Lett.* **1994**, *72*, 3389.
(52) Cavalleri, A.; Dekorsy, T.; Chong, H. H. W.; Kieffer, J. C.; Schoenlein, R. W. *Phys. Rev. B.* **2004**, *70* (16), 161102.

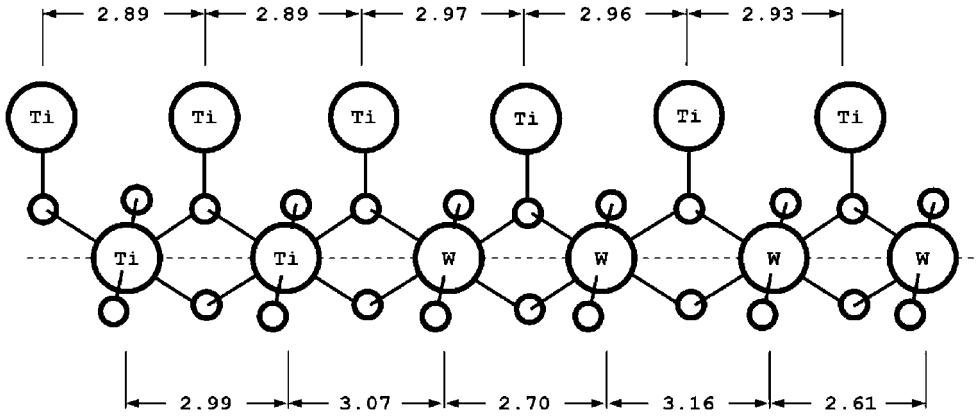

Figure 7. Unit-cell schematic of $[Ti_{0.67}W_{0.33}O_2]_{12}$ after annealing simulations and optimization.

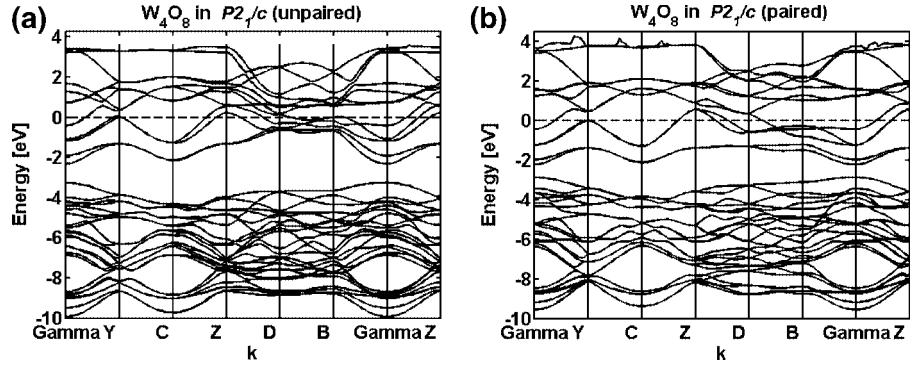

Figure 8. Band structure of $[WO_2]_4$ in space group $P2_1/c$: (a) unpaired, (b) paired.

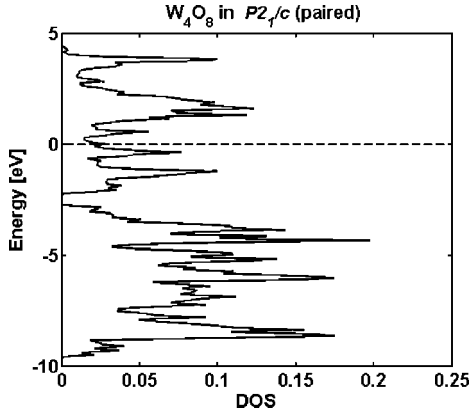

Figure 9. Density of states around the Fermi level for $[WO_2]_4$ in space group $P2_1/c$ or the reoptimized crystal (paired) after 100 steps of annealing MD.

formula units. In Figure 5, two unit cells are shown for the $P2_1/c$ and $P4_2/mnm$ alternative space groups. Calculations for the two models in Figure 5 were performed using both the VASP[37−39] and the Quantum-ESPRESSO[53] codes (using one as a check for the other). In the DFT calculations by the latter software, pseudopotentials W.pw91-nsp-van.UPF and Os-pw91-n-van.UPF were used.

The results are presented in Table 2. First consider the $P2_1/c$ starting structure, for which DFT lattice parameters, although slightly larger, are on average close enough to the experimental measurements so one can trust the calculations. The W−W pairing is clear (see last two rows for distances along the chain); the shorter metal−metal bond length is approximately 0.5Å different from the longer one, with each method of calculation. In contrast, for WO_2 in the $P4_2/mnm$ (rutile) structure, no pairing is suggested by the standard stability criterion. The first morphology, $P2_1/c$, is more stable than the second by 0.325 eV per WO_2 unit.

We were bothered by the absence of pairing for WO_2 when it was computed in the rutile space group. Perhaps the computations are getting stuck in a local minimum, or the space group constraints do not allow the pairing to happen. One way to overcome this is to increase the temperature of the model system and thereby simulate an annealing process (to which real materials are exposed during synthesis). Among the wide range of available methods and simulation parameters, we chose to perform Car−Parrinello[54] ab initio molecular dynamics (MD) implemented in the VASP code. The initial temperature of the system was increased to 600 K, and a final temperature of 300 K was requested. The total number of simulation steps was 100, each 3 fs long. The calculated temperature profile is plotted in Figure 6. During about 40% of simulation time, the system experienced fluctuating temperatures higher than the linear profile; at some points as high as 1000 K.

Temperature fluctuations did introduce short and long bond lengths along metal chains, whose pairing pattern was retained by a follow-up optimization step. As seen from

(53) Baroni, S.; Dal Corso, A.; de Gironcoli, S.; Giannozzi, P.; Cavazzoni, C.; Ballabio, G.; Scandolo, S.; Chiarotti, G.; Focher, P.; Pasquarello, A.; Laasonen, K.; Trave, A.; Car, R.; Marzari, N.; Kokalj, A. http://www.pwscf.org/.

(54) Car, R.; Parrinello, M. *Phys. Rev. Lett.* **1985**, *55*, 2471.

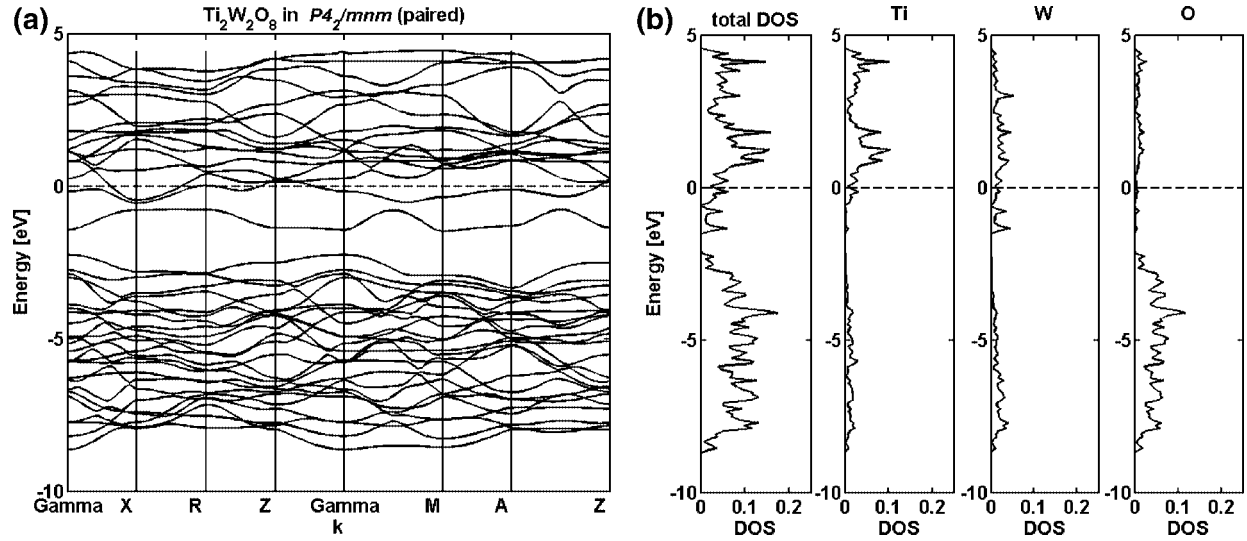

Figure 10. $[Ti_{0.5}W_{0.5}O_2]_4$ in space group $P4_2/mnm$ reoptimized crystal (paired) after 100 steps of annealing MD: (a) band structure, (b) density of states.

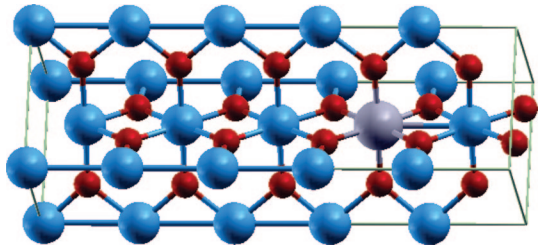

Figure 11. Unit cell used for the 10% W doping model. The largest atom in the metal chain is W.

Table 2, the difference between the short and long bond lengths is about 0.42 after the last MD step and about 0.48 after final unit-cell optimization. Both values are slightly smaller than the difference in the paired $P2_1/c$ structure in Table 1. The paired $P4_2/mnm$ system (no longer in this space group when paired, but we find it useful to refer to it by the parent structure) is more stable than the unpaired by 0.3 eV per unit cell, but still 1.1 eV higher in energy than $P2_1/c$.

Although the computational approach is seen to provoke pairing (and with it stabilization) for WO_2 in the rutile structure, the more stable WO_2 structure is not reached; perhaps the temperature or perturbations are not sufficiently high. We now return to rutile to investigate pair formation upon W-doping.

6. W-Doped Rutile

Two doped structures were revisited on the basis of our findings on stoichiometric WO_2 in the rutile structure: 33% (case I), and 50% (case II). The unit cell is once more doubled to allow short and long distances to occur. Also, working from the same interest in allowing any potential pairing to manifest itself, the doped chain is taken as $-[TiTiWWWW]_n-$ rather than the simply doubled $-[TiWWTiWW]_n-$. In each case, two sets of calculations are performed: (i) a conventional optimization of lattice parameters, and (ii) an annealing MD simulation followed by a final cell optimization (see Table 3. Corresponding results are given in Table 4. In case I, a paired structure is observed not only after the MD annealing but early on in the optimization-only calculations too. Thus there is essentially no energy difference between the two final structures. A schematic drawing of the distances in the paired chain for 33.3% doping is given in Figure 7.

In case II, however, long and short distances are formed only after the system undergoes heat treatment. The relative stability of the annealed paired system (−0.36 eV) also reflects significant difference between those structures. One might have expected that the doping-initiated pairing should have occurred earlier and stronger in the highly doped case II than in less doped case I. This did not happen; a cautionary lesson here about the need to avoid getting stuck in artificial minima because of undetected constraints in optimization.

7. Pairing and Doping Effects on Electronic Structure

Comparing the two models in section 5, we see the same octahedral environment. Burdett and Whangbo have given us the general reasons one might expect pairing; essentially, W−W bond formation, a Peierls distortion, driven by occupation of bonding σ and π bands.[6,49,55,56] In his comprehensive paper on stabilities and distortions in rutile-type structures, Burdett explicitly analyzes MoO_2 and more generally concludes that the metal−metal interaction in the rutile structure is strongest for d^2 and d^3 configurations. Whangbo and Foshee[48] address the alternating bonds in NbX_4 chains, a system quite similar to WO_2. Though the d-electron count is different, interestingly, they obtain a difference between the long and short bonds of 0.36 Å, not very different from what we calculate for WO_2.

Can we find support for this qualitative picture in the band structure calculations? Let us begin in the $P2_1/c$ WO_2 structure by first constructing a model in which the pairing is removed, the tungsten atoms distributed at equal distances. The lower 24 bands (see Figure 8) are O(2p) levels on 8 oxygen atoms. All the valence bands close to the Fermi level

(55) Englman, R. *Jahn-Teller Effect in Molecules and Crystals*; John Wiley & Sons Ltd.: London, 1972.
(56) Wheeler, R. A.; Whangbo, M. H.; Hughbanks, T.; Hoffmann, R.; Burdett, J. K.; Albright, T. A. *J. Am. Chem. Soc.* **1986**, *108* (9), 2222–2236.

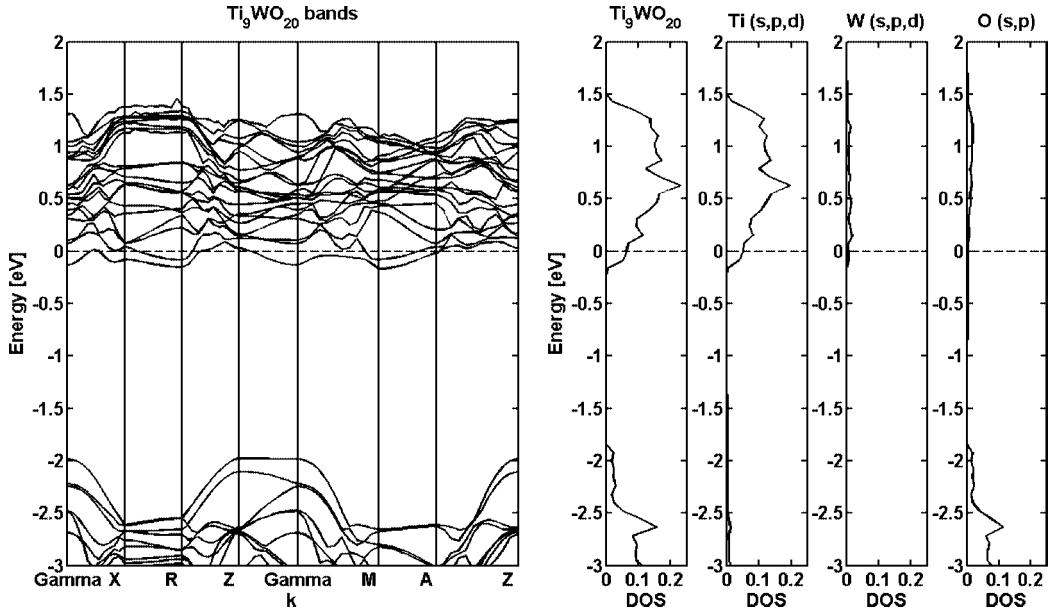

Figure 12. (left) Band structure of $[Ti_{0.9}W_{0.1}O_2]_{10}$, (right) its DOS, with atom projections.

(ε_F) are dominated by states based on W(5d) orbitals. The levels were identified by a Maximally Localized Wannier Functions analysis.[57] These levels are very similar to each other in the paired and unpaired structures.

Notice the difference of those d-states around ε_F from D to B, the two corners of the Brillouin zone in the paired and unpaired crystals. Clearly, some degeneracy and cluttering of levels in the unpaired geometry has been eliminated by pairing of metal−metal atoms. Some levels have moved above, some below the Fermi level, a typical consequence of bond formation. The stability of paired metal chains is also reflected in lowering of the Fermi level by about 0.2 eV. Electronic stabilization as a consequence of reducing the translational symmetry of the crystal, or electron−phonon coupling, was first suggested by Peierls.[55] A chemical account is given by Burdett, and by Whangbo, with specific applications to the system at hand.[48,49]

Now let us return to WO_2 and W-doped rutile in their paired and unpaired structures. Similar electronic consequences of pairing emerge there. The total DOS (see Figure 9) indicates that despite the pairing, the density of states at the Fermi level for WO_2 is indicative of metallic behavior, consistent with what is known for the material.

Next we show the band structure and DOS for the paired structure (after MD annealing) of the 50% doped model (see Figure 10). The levels around the Fermi level are mainly W(5d) in character (again judging from the Wannier analysis), and the material is conducting, as anticipated.

We also calculated a model for 10% W doping; the structure assumed had all Ti in one chain, one out of five Ti replaced by W in the other, as shown in Figure 11. The computed band structure and DOS is illustrated in Figure 12.

The Fermi level is now located near the bottom of the t_{2g} band. The projections of the DOS show that there is a contribution of both Ti and W levels to the DOS near the Fermi level. At the Fermi level, the contribution to the DOS from Ti is 81%, and from W 9%. There are 9 times as many Ti as W in the unit cell. This suggests that the electrons on the W spread out onto surrounding Ti atoms and that the conducting states near the Fermi level are moderately delocalized around the W. Thus a band model rather than a percolation model of W-to-W electron hoping is the appropriate picture to describe the conductivity of these doped metals. The 50% Ti/W doped model is roughly isoelectronic with VO_2, on which there is a substantial literature.[58−61] In VO_2, the same questions of pairing arise. There, the atoms are equivalent, whereas our model simulates ordered doping, with resulting asymmetry.

8. Conclusion

In this work, we studied doping the rutile structure with tungsten, because of the potential of the doped material as a catalyst support in industrial applications such as fuel cells. In accord with experimental measurements, we found that upon tungsten doping, some of the structural (lattice parameters) and electronic (conductivity) properties of rutile change in noticeable ways. Pure WO_2 crystallizes in space group ($P2_1/c$); calculations are in accord with this. Pairing of W atoms is evident in the structure. Molecular dynamics is needed to initiate the tendency to pair W atoms in WO_2 if the latter is optimized in the $P4_2/mnm$ rutile structure.

In both structural types, W−W pairing clears up some but not all of the cluttering of bands around the Fermi level.

(57) Marzari, N.; Vanderbilt, D. *Phys. Rev. B* **1997**, *56*, 12847.

(58) Biermann, S.; Poteryaev, A.; Lichtenstein, A. I.; Georges, A. *Phys. Rev. Lett.* **2005**, *94*, 026404.

(59) Eyert, V.; Horny, R.; Hock, K. H.; Horn, S. *J. Phys.: Condens. Matter* **2000**, *12*, 4923–4946.

(60) Zylbersztejn, A.; Mott, N. F. *Phys. Rev. B* **1975**, *11*, 4383–4395.

(61) Koethe, T. C.; Hu, Z.; Haverkort, M. W.; Schussler-Langeheine, C.; Venturini, F.; Brookes, N. B.; Tjernberg, O.; Reichelt, W.; Hsieh, H. H.; Lin, H.-J.; Chen, C. T.; Tjeng, L. H. *Phys. Rev. Lett.* **2006**, *97*, 116402.

The material remains metallic. The states directly below and above the Fermi energy emerge as mainly metal-based, W(5d). Metallicity is retained in the W-doped TiO_2 structure, both at high and low doping levels.

Acknowledgment. This work was supported by the Office of Science, Department of Energy, through a grant to the Cornell Fuel Cell Institute: DE-FG02-03ER46072. Some calculations in this work have been done using the Quantum-ESPRESSO package.[53]

Supporting Information Available: Additional band structure figures (PDF). This material is available free of charge via the Internet at http://pubs.acs.org.

CM900329K